Coupling CO_2 electrolysis and downstream processing via heat pump-based waste heat recovery

Dal Mas, Riccardo; Carta, Andrea; Somoza-Tornos, Ana; Kiss, Anton A.

DOI
10.1016/j.compchemeng.2025.109330

Publication date
2026

Document Version
Final published version

Published in
Computers and Chemical Engineering

Citation (APA)
Dal Mas, R., Carta, A., Somoza-Tornos, A., & Kiss, A. A. (2026). Coupling CO_2 electrolysis and downstream processing via heat pump-based waste heat recovery. *Computers and Chemical Engineering*, *204*, Article 109330. https://doi.org/10.1016/j.compchemeng.2025.109330

Computers and Chemical Engineering 204 (2026) 109330

Contents lists available at ScienceDirect

Computers and Chemical Engineering

journal homepage: www.elsevier.com/locate/compchemeng

Coupling CO_2 electrolysis and downstream processing via heat pump-based waste heat recovery

Riccardo Dal Mas, Andrea Carta, Ana Somoza-Tornos, Anton A. Kiss *

Department of Chemical Engineering, Delft University of Technology, Van der Maasweg 9, 2629 HZ Delft, the Netherlands

ARTICLE INFO

Keywords:
Heat pumps
CO_2 electrolysis
Downstream processing
Waste heat recovery

ABSTRACT

The electrification of chemical processes and CO_2 utilization are key approaches to improving efficiency and reducing CO_2 emissions in the process industry. The development of electrolyzers has gathered momentum, enabling the potential introduction of renewable electrons into the manufacture of CO_2-based chemicals. While the performance of electrolyzers is subject to improvements driven by the experimental community, the generation of waste heat is unavoidable due to electrical resistances and process inefficiencies within the electrochemical cells. Nonetheless, reusing this waste heat has yet to be investigated for CO_2 electrolyzers. This novel work shows the potential for upgrading the electrolyzer waste heat by means of a heat pump, enabling its utilization in the separation processes downstream of the carbon dioxide electrolyzer. The product chosen is formic acid (60 kt/y), and for our system, the waste heat represents approximately 60 % of the power input to the electrochemical cells, and it can be upgraded from 50 °C to 120 °C to drive the azeotropic distillation of formic acid and water. This integration results in the electrification of 76 % of the separation energy duty, yielding a decrease in CO_2 emissions of 29–84 % compared to the conventional production, depending on the source of electricity. The results demonstrate that the use of traditional heating media in thermal separation processes can be offset and substituted with (renewable) electrical energy, allowing for an increased overall system efficiency. This approach can be readily extended to different productions based on carbon dioxide electroreduction, for example for methanol and ethanol manufacture. This eco-efficient process design leads to a deeper penetration of renewable energy into chemical manufacturing, as both reaction and separation are driven by electricity.

1. Introduction

Electrification and carbon dioxide utilization are recognized as fundamental strategies to improve the environmental performance of chemical processes and advance the industry towards its decarbonization targets (Mallapragada et al. 2023; Zhao et al. 2023). In particular, low-temperature carbon dioxide electrolysis combines the two approaches, exploiting (renewable) electricity to drive the conversion of carbon dioxide into useful products (De Luna et al. 2019). However, this is a generally inefficient process due to ohmic and kinetic losses (Zhang, Xie, and Wang 2022), which translate into waste heat generation (Van Der Roest et al. 2023). This waste heat offers a potential for energy integration, even though its low temperature limits possible applications. To expand the use cases, heat pumps can be deployed, raising the temperature level of the heat and allowing for its utilization (Schlosser et al. 2020). Moreover, mechanically driven heat pumps are also based on electricity inputs, thus furthering the substitution of conventional fossil-based energy with (renewable) electrical one (Kiss and Smith 2020).

Low-temperature carbon dioxide electrolysis has seen major advancements in recent years, driven by the experimental community (O'Brien et al. 2024), with contributions from Process Systems Engineering via techno-economic and life-cycle assessments (Somoza-Tornos et al. 2021). However, the problem of operating temperature and waste heat management in the electrolyzers is largely unexplored: most experimental setups are operated at room temperature, with fewer examples of experiments carried out at higher temperatures (Lee et al. 2018; Hu et al. 2023), while other studies investigate the effects of temperature on the cell performance (Kibria et al. 2019; Gabardo et al. 2019; Vos and Koper 2022; Vos et al. 2023). The findings show positive effects of higher operating temperatures on current densities, owing to increased conductivity and faster reaction kinetics, and Hurkmans et al. (2025) show that an optimal operating temperature for the reactor lies between 60 and 70 °C. Notably, this range is similar to the operating temperature reported for water electrolyzers (both PEM (Bonanno et al.

* Corresponding author.
E-mail address: A.A.Kiss@tudelft.nl (A.A. Kiss).

https://doi.org/10.1016/j.compchemeng.2025.109330
Received 30 April 2025; Received in revised form 21 July 2025; Accepted 7 August 2025
Available online 8 August 2025

Notations and abbreviations

CAPEX	Capital Expenditure
COP	Coefficient of Performance
OPEX	Operational Expenses
PEM	Proton Exchange Membrane
VCHP	Vapour Compression Heat Pump
VHC	Volumetric Heating Capacity

2024) and alkaline (Zhang et al. 2024)).

Among the products of carbon dioxide electrolysis, liquid products present specific process challenges due to the dilute nature of the electrolyzer product stream, which translates into significant energy demands for their separation (30–85 % of the total process requirements) (Kibria Nabil et al. 2021; Orella et al. 2020). Since most separation technologies are thermally-driven (Kiss and Smith 2020), and process heat is mostly fossil-based (IEA 2024), these processes would incur significant emissions, thus undermining their advantages compared to conventional productions (Kibria Nabil et al. 2021). One strategy to address this issue is to increase the concentration of the product streams without compromising the reactor efficiency, but this is still an open challenge (Zhu and Wang 2021). Alternatively, process technologies can be devised to improve the separation performance, as Barecka et al. (2023) have done for ethanol. However, given the availability of large amounts of waste heat from the electrolyzers, energy integration can be performed by coupling the upstream energy output with the downstream energy demand via a heat pump. In this work, we demonstrate by developing a techno-economic assessment that this can lead to a substitution of the external heat supply with (renewable) electricity, resulting in environmental and economic advantages for the overall system. As the heat pump performance is dependent on the source (the electrolyzer) and the sink (the downstream) temperatures, our work also highlights the additional benefit on the overall process of increasing the electrolyzer operating temperature (in the range from 50 to 70 °C).

Heat pumps are used to improve the efficiency of industrial processes (Schlosser et al. 2020; Jiang et al. 2022), and while their penetration in the industry is still relatively modest, their possible impact is recognized (Madeddu et al. 2020). Their application to waste heat upgrade from low temperature electrolysis has been explored in the works of Van Der Roest et al. (2023) and Galvan-Cara and Bongartz (2025) with respect to hydrogen production. In our work, we extend this concept to carbon dioxide electrolysis processes, selecting, as a case study, the production of formic acid. This is a product readily obtained via carbon dioxide electrolysis (Fernández-Caso et al. 2023), and is of interest in the chemical industry, albeit with a comparatively smaller market (~1 Mt/y) with respect to other base chemicals (Hietala et al. 2016), even though new applications, in particular as an energy storage medium, might expand it in the future (Thijs et al. 2022; Chatterjee et al. 2021; Crandall et al. 2023). The interest in formic acid is also evidenced by the number of process designs and techno-economic assessments for its manufacturing from carbon dioxide, including both thermochemical hydrogenation (Pérez-Fortes et al. 2016; Kalmoukidis et al. 2024; Kim et al. 2024), and low temperature electrolysis (Rumayor et al. 2019; Ramdin et al. 2019; Rumayor, Dominguez-Ramos, and Irabien 2019).

Moreover, while high energy efficiency for the electrolyzer is generally recognized as a fundamental requirement for the competitiveness of carbon dioxide electrolysis processes (Martín et al. 2015), our energy-integrated process allows for a broader investigation. Specifically, we explore the system-wide trade-off between cell efficiency and external heat supply. In fact, we can identify through a multi-objective optimization the operating conditions for the electrolyzers that lead to the best economic and environmental performance for the overall system. These conditions are dependent on wider techno-economic assumptions, namely the price and source (renewable versus grid) of the electricity inputs.

Within this paper, we first describe the process design for the conversion of carbon dioxide to formic acid, basing the electrolyzer design on experimental data and the separation process on designs from the literature (Yang et al. 2020; Ramdin et al. 2019). Energy integration is performed via a mechanically-driven heat pump – a technology not yet explored in the context of carbon dioxide electrolysis processing – and we include a screening of different working fluids and conditions, evaluating the techno-economic and environmental advantages of the integrated system. We benchmark this against the conventional formic acid production based on fossil resources, as well as literature studies for its manufacture from carbon dioxide. The analyses are compounded by process optimization under different conditions, offering additional and novel perspectives into the behaviour of the carbon dioxide electrolysis process to liquid products.

2. Methodology

This section presents the methodology used to design and size each part of the process, followed by the presentation of the economic and environmental metrics utilized. Finally, the optimization of the process is introduced.

The process is composed of three main parts, as shown in Fig. 1: the electrolyzers, the downstream separations, and the heat pump. The electrolyzers and downstream are connected via mass flows, while the heat pump integrates the process sections through energy exchanges, recovering and upgrading the waste heat from the electrolyzer to provide it to the separations. The steady state process was designed and simulated in Aspen Plus®, sizing the plant for an industrially-relevant capacity (60 kt/y of FA at 85 wt %, with 8000 h/y of operation).

2.1. Electrolyzer

A three-compartment reactor based on the work of Yang et al. (2020) (Dioxide Materials, 2024) was selected for this study. This system, shown schematically in Fig. 2, was chosen due to its overall good performance and its simplicity, since it does not include additional electrolytes and produces directly a solution of formic acid, eliminating the need for further ionic separations. The cell is fed with deionized water on both the anode and middle compartments, while the cathode receives a gaseous stream of carbon dioxide. The main (overall) reaction is given in Eq. (1), whereas secondary reactions lead to the formation of hydrogen and carbon monoxide (Eqs. (2) and (3), respectively). Formic acid leaves the cell from the middle compartment, while the gaseous by-products leave with the unreacted carbon dioxide stream.

$$CO_2 + H_2O \rightarrow HCOOH + 0.5\ O_2 \quad (1)$$

$$H_2O \rightarrow H_2 + 0.5\ O_2 \quad (2)$$

$$CO_2 \rightarrow CO + 0.5\ O_2 \quad (3)$$

The key performance metrics considered for this study include cell voltage, current density, Faradaic efficiencies, and temperature. The polarization curve was obtained from experimental data reported in Yang et al. (2020), as well as the effect of the middle compartment flow on the Faradaic efficiencies (see *Supplementary Information* for more details). The availability of data limits the cell voltage range considered to 2.3–4 V.

The total current i and power input P to the electrolyzers are calculated based on Eqs. (4) and (5), where R is the production rate of formic acid, z is the number of electrons per mole of product, F is the Faraday constant, FE is the Faradaic efficiency towards the product, and E_{cell} is the cell voltage. The dependency of the current density on the cell voltage is captured thorough the fitted polarization data, and it is used to evaluate the power requirements and electrolyzer area at scale.

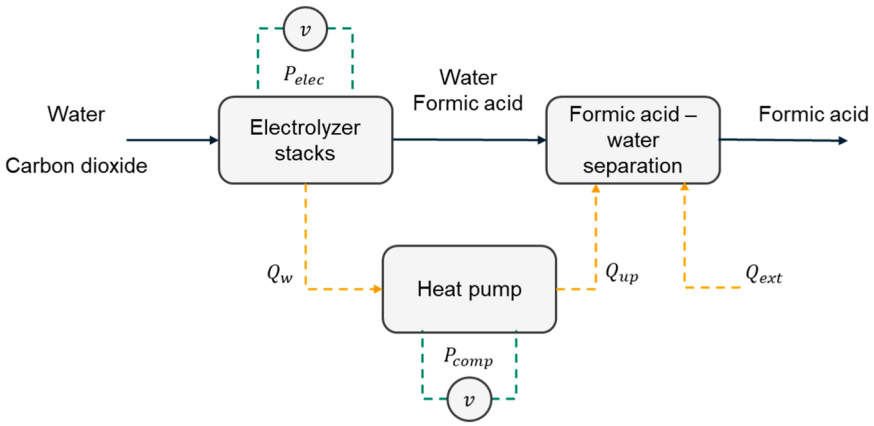

Fig. 1. Block flow diagram for the process, showing the three main process components (electrolyzers, downstream separations, and heat pump). The main energy streams are also shown, with the electricity inputs in green and thermal energy flows in orange.

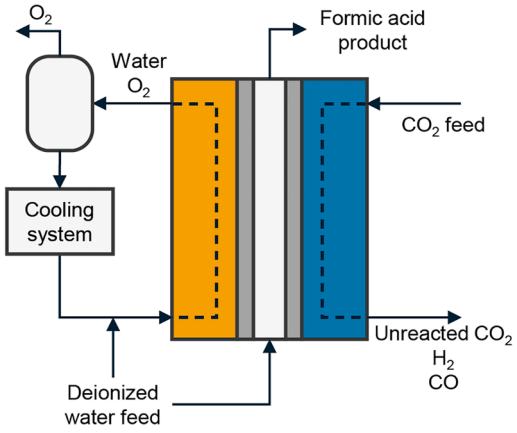

Fig. 2. Simplified scheme of a three-compartment cell for the reduction of carbon dioxide to formic acid (based on Yang et al. (2017)). The cell comprises an anodic side, in orange, where water is oxidized to oxygen; a middle compartment, in grey, where the formic acid product is collected; and a cathodic side, in blue, where CO_2 is reduced to formic acid.

$$i = \frac{R}{z\ F\ FE} \tag{4}$$

$$P = i\ E_{cell} \tag{5}$$

The thermoneutral voltage $E_{th,k}$ (for product k) is the value of the voltage at which the cell dissipates no heat, as the heat developed by the system inefficiencies and overpotentials balances the heat required by the endothermic reactions (Harrison et al. 2010). This value was used to evaluate the performance of the electrolysis step through the energy efficiency, as defined in Eq. (6), where, FE_k is the Faradaic efficiency for product k, and E_{cell} is the total cell voltage, with the voltages calculated at standard conditions (Martín et al. 2015).

$$\varepsilon = \frac{\sum_k E_{th,k} FE_k}{E_{cell}} \tag{6}$$

The thermoneutral voltage is also used to estimate the thermal power dissipated by the electrolyzers, calculated as the product of the total cell current and the difference between the cell voltage and the thermoneutral voltage, as given in Eq. (7) (Van Der Roest et al. 2023), where i_k is the partial current for product k ($i_k = FE_k i$, with i total current).

$$Q_w = \sum_k i_k \left(E_{cell} - E_{tn,k}\right) \tag{7}$$

The performance of the electrolyzer was selected based on an economic trade-off between the calculated capital and operational expenditure (see Section 2.4), selecting the cell voltage value corresponding to the minimum of the total costs. The design of the electrolyzer was carried out first in a stand-alone way for the base case design of the process, and it was then revisited within the process-wide optimization based on the energy integration of the process.

The electrolyzer model was first implemented in Python for detailed design, and then in Excel to embed it within Aspen Plus as a User2 custom model. The thermodynamic package of choice for this part of the flowsheet is ELECNRTL, as this can account for the dissociation of formic acid in water and presents built-in binary interaction parameters for the system of interest (Aspen Technology, Inc. 2013).

Note that the model of the electrolyzer is based on data collected at room temperature, which are applied to a cell assumed to be operated at higher temperatures. Temperature difference could affect both the activity and the selectivity in the system, and on one hand the polarization curve of the system could change as kinetics, conductivities, and resistances are functions of temperature. On the other hand, the equilibrium and thermoneutral potentials are not significantly affected by changes in temperature (see *Supplementary Information*), thus corroborating the use of Eq. (7). Moreover, the electrolyzer has been scaled up linearly based on the performance of the lab-scale equipment, assuming that the flow rates in the different compartments scale with the area of the equipment. Likewise, the current density versus voltage curve, as well as the effect of the middle compartment flow on the Faradaic efficiencies, are set not to change as the area is increased. This approach does not capture potential scale-up issues with respect to mass transport limitations or increased ohmic losses: these would affect the various overpotentials and ultimately the cell voltage-current density relationship (Wakerley et al. 2022; Salvatore and Berlinguette 2020; Goldman et al. 2023).

2.2. Downstream separation

The electrolyzer outlet is a diluted aqueous mixture of formic acid, which presents a maximum boiling point azeotrope (Hietala et al. 2016). The separation of this mixture, studied mostly within the context of conventional production routes, can be accomplished via extractive distillation (Ge et al. 2023), pressure swing distillation (Chua et al. 2019; Mahida et al. 2021), or several intensified technologies (Sharma et al. 2018; Da Cunha et al. 2018). Ramdin et al. (2019) also discuss the production of formic acid via carbon dioxide electroreduction, and they discourage the use of distillation for the separation of diluted aqueous formic acid streams (<10 wt %), due to the large amount of water to be removed. The solution they propose is a combination of extraction using a low-boiling solvent, namely 2-methyltetrahydrofuran (2-MTHF), followed by azeotropic and vacuum distillation to recover the product, and

finally by a stripper to recycle the solvent. In addition, 2-MTHF can be sourced renewably from biomass and has been described as a green solvent (Bangalore Ashok et al., 2022; Pace et al. 2012). Moreover, to maximize the performance of the heat pump in the integrated process, a key consideration in the design of the separation process is the temperature at which energy is supplied, which should ideally be as low as possible. We chose this separation scheme, a detailed description of which is provided in the *Supplementary information*, because of the low process temperature, use of a green solvent, and removal of the bulk of the water from the electrolyzer outlet stream through the extractor. As a thermodynamic model, NRTL-HOC is used, despite most previous works on this system using UNIQUAC—HOC, as it has been shown that the former has better performance for this system (Ramdin et al. 2019), and the binary interaction parameters for the three binary pairs (formic acid, water, 2-MTHF) reported in their work are used for the simulation.

Alongside the liquid separation, the downstream includes the recovery of unreacted carbon dioxide from the cathodic stream, as well as the separation of the hydrogen and carbon monoxide generated as byproducts. This is done via high pressure multi-stage condensation of the carbon dioxide, achieved with several compressor stages with intercooling.

2.3. Heat pump

Several heat pump technologies can be integrated into chemical processes (Kiss and Infante Ferreira 2016), and, specifically, mechanically-driven heat pumps can increase the penetration of (renewable) electricity in chemical processes. Consequently, vapor compression heat pumps (VCHP), using pure fluids, have been selected as the technology of choice (Van De Bor et al. 2014). The heat pump is schematically represented in Fig. 3, which shows how the heat pump upgrades the waste heat at low temperature Q_w to a heat stream at high temperature Q_{up} (Walden et al. 2023), which is approximately equal to the sum of the waste heat and the power input to the heat pump compressor P_{comp} (Eq. (8)). The heat pump performance improves as the compressor power required to upgrade the waste heat to the desired temperature level decreases, and this is measured by the Coefficient of Performance (*COP*), defined in Eq. (9). This key performance indicator is used, together with the Volumetric Heating Capacity (*VHC*), expressed by Eq. (10) (Frate et al. 2019) to guide the techno-economic screening of the heat pump.

$$Q_{up} \cong Q_w + P_{comp} \tag{8}$$

$$COP = \frac{Q_{up}}{P_{comp}} \tag{9}$$

$$VHC = \frac{Q_{up}}{V_{comp,in}} \tag{10}$$

Several working fluids were screened and evaluated based on the thermodynamic and environmental performance (data reported in the *Supplementary Information* (Frate et al. 2019; Wu et al. 2020; Arpagaus et al. 2018)). The simulation tunes the pressures after the expansion and the compressor to match the required temperature levels for heat exchange in the evaporator (electrolyzer cooler) and in the condenser (column reboiler), as well as the working fluid flow rate, to ensure that the heat exchanged matches the requirements for the electrolyzer cooling. The temperature approach has been set to 5 K. The electrolyzer is assumed to be operating at 50 °C, with a return temperature of 10 K lower: to study the effects of the electrolyzer temperature on the system, we have evaluated the heat pump performance for electrolyzer temperatures up to 70 °C. The compressor was modelled as isentropic with isentropic and mechanical efficiencies of 85 and 98 %, respectively. The heat pump has been modelled in Aspen Plus®, employing the REFPROP thermodynamic package, which implements fundamental equations of state for specific refrigerants (Lemmon et al. 2018). REFPROP utilizes the most accurate models for pure fluids and mixtures, as detailed in Huber et al. (2022) and Aspen Technology, Inc. (2013).

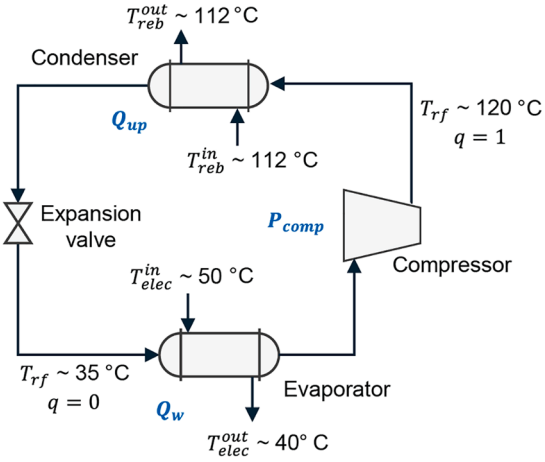

Fig. 3. Process scheme for a vapor compression heat pump. The subscript *rf* refers to the working fluid, while *elec* and *reb* refer to the process side streams in the electrolyzer cooler and the column reboilers, respectively. The temperature values are discussed in the Results section.

2.4. Economic and emissions assessment

A techno-economic assessment for the process was developed to establish its economic feasibility. The heat pump is not an integral part of the formic acid manufacturing process, and, therefore, it was treated as an add-on module compared to the case without heat integration, used as a benchmark to evaluate the possible advantages of the heat pump. This second case uses external thermal energy inputs, based on medium pressure steam. The levelized cost of production of formic acid *LCFA*, defined in Eq. (11), was taken as the main economic performance metric for the process. The levelized cost is evaluated based on an economic allocation of the cost to the products, considering the percentage of revenues attributable to the product. The payback period (Eq. (12)) was used to evaluate the economic advantages of the heat pump under different cost scenarios for electricity and fuel.

$$LCFA = \frac{Annualized\ CAPEX + OPEX}{Production} \cdot Percentage\ of\ revenues\ from\ FA \tag{11}$$

$$Payback\ period = \frac{CAPEX_{HP}}{Net\ cash\ flow} \tag{12}$$

To determine the Operating Expenditure (OPEX), we considered the raw material consumption and the utilities demands, with the carbon dioxide price based on point source capture (Bains et al. 2017). The capital expenditure (CAPEX) was estimated using the methods of Sinnott and Towler (2020), except for the electrolyzer stacks, with costs evaluated based on the total area of the units. The CAPEX was annualized over the 20-year plant lifetime, assuming a 10 % interest rate. The compressor is typically the most expensive unit in the heat pump (Vannoni et al. 2023); however, there is a lack of consistency in the costing estimation for compressors (Luyben 2018). Therefore, we have considered different CAPEX calculation methods for the compressor, with the results reported in the *Supplementary Information*. This also includes the values of the inputs needed for the economic estimation, which were varied by ±30 % to perform a sensitivity analysis.

Product sales, necessary for the economic allocation of the costs to the product, include formic acid (85 wt %) and by-product syngas, comprising primarily hydrogen. As the syngas composition depends on the design, its price is based on the heating value and the composition obtained (Alerte et al. 2023). Oxygen, albeit of potential interest as a

by-product, is not considered as such, since it is typically vented in electrolysis processes (Kato et al. 2005; Eckl et al. 2025).

We have estimated the scope 1 and 2 carbon dioxide emissions per unit product e_{CO_2} (Bauer et al. 2023), which derive from energy supplied to the process and its origin. This metric is calculated using Eq. (13), where Q_{th} and Q_{el} are the total process demands (in kWh/y) for thermal and electrical energy, respectively, CI_{th} and CI_{el} are the carbon intensities (in gCO_{2eq}/kWh) of thermal and electrical energy, respectively, and finally P_{Prod} is the total production of formic acid (in kg/y). The carbon dioxide emission value supports and provides context for the decisions on design and the benefits of upgrading the waste heat by means of the heat pumps. The energy supplies considered are electricity from a grey grid (251 gCO_{2eq}/kWh, based on EU-27 average (European Environment Agency, 2025)), from offshore wind (19 gCO_{2eq}/kWh (U.S. Department of Energy 2015)), and thermal energy provided by medium pressure steam (259.2 gCO_{2eq}/kWh (Pérez-Fortes et al. 2016)). The process does not have direct carbon dioxide emissions, since the unreacted feed is either recycled or sold as part of the syngas by-product.

$$e_{CO_2} = \frac{Q_{th}\, CI_{th} + Q_{el}\, CI_{el}}{P_{Prod}} \tag{13}$$

Scope 3 emissions, including the impact of upstream production of raw materials (refrigerant, solvent) and supply chain effects (carbon dioxide capture and transport), as well as the calculation of other metrics typical of a Life Cycle Assessment, are beyond the scope of the current conceptual design. The results of the emissions have been compared with those obtained from the conventional production of formic acid via the methyl formate route, obtained from SimaPro using the Ecoinvent 3.8 (2021) (Wernet et al. 2016) system database at the point of substitution and the ReCiPe 2016 method (with Midpoint (H) level characterization factors) (Huijbregts et al. 2017).

2.5. Optimization

The integrated process involves multiple trade-offs, the most significant one being the relationship between cell voltage and global system efficiency, measured both in terms of cost and emissions. In fact, lowering the cell voltage improves cell efficiency, but results in less waste heat available, thus increasing the need for external thermal energy inputs for the separation. As a consequence, the process would produce higher carbon dioxide emissions, especially if compared to the case with a larger heat pump powered by renewable electricity. Conversely, lower waste heat generation can reduce the size, and thus the cost, of both the heat pump compressor and the heat exchangers due to the use of utilities with higher temperature driving forces.

To formally address this trade-off, we set up a multi-objective optimization to find the optimal plant operating conditions that minimize both the total annualized cost and the carbon dioxide emissions. In this study, we considered a single decision variable, the cell voltage, varied in the validated range of 2.3–4 V. This modeling choice reflects our focus on analyzing heat integration in the process, while leaving the inclusion of additional decision variables to future work on broader process optimization. A constraint on the total production of formic acid was imposed. The objective functions for total cost (Eq. (14)) and CO_2 emissions (Eq. (15)) are defined below, where the subscripts *elec*, *HP*, and *ext* refer to the electrolyzer, the heat pump, and the external cooling/heating system, respectively, while *comp* and *HEX* refer to the compressor and to heat exchangers, respectively. We built the objective function to include the cost factors affected by the decision variable. Note that the downstream separation and CO_2 recovery remain unchanged by the optimization, thus we omitted them from the calculation (Eq. (14)).

$$obj_1 = \frac{CAPEX_{elec}}{lifetime_{elec}} + \frac{CAPEX_{HP,comp} + CAPEX_{HP,HEX} + CAPEX_{ext,HEX}}{lifetime_{plant}} + OPEX_{elec} + OPEX_{HP} + OPEX_{ext} \tag{14}$$

$$obj_2 = \frac{\left(Q_{el,elec} + Q_{el,HP}\right)\cdot CI_{el} + Q_{th,ext}\cdot CI_{th}}{P_{Prod}} \tag{15}$$

To investigate the effect of varying operating conditions, we ran the optimization with different electricity prices (0.05–0.1 $/kWh) and sources (renewable or grid).

The multi-objective optimization was performed by applying the ε-constraint method (Mavrotas 2009), implementing the model in Python (version 3.11.4), using the Sequential Least Squares Programming (SLSQP) optimization method (Kraft 1988). Further details on the implementation, including a flow chart for the solution procedure, can be found in the *Supplementary Information*.

3. Results and discussion

In this section, we present and discuss the results for the electrolyzer design, followed by the heat pump sizing, including the working fluid selection and the impact of the electrolyzer temperature on its performance. Subsequently, we describe the full, energy-integrated process and its techno-economic and environmental performance, benchmarking it to the case without the heat pump and comparing it to results from the literature. Finally, the insights from the optimization are evaluated under different scenarios of electricity price and source.

3.1. Electrolyzer design and energy balance

The choice of the operating conditions for the electrolyzer is based on the trade-off between OPEX and CAPEX displayed in Fig. 4a, which shows a behaviour consistent with that observed in similar systems for carbon dioxide electrolysis (Masel et al. 2021; Berkelaar et al. 2022). For the base case values of 0.05 $/$kWh_{el}$ and 1500 $/m^2 for electricity price and electrolyzer cost, respectively, the value of the cell voltage which minimizes the total cost falls at ~3.3 V, corresponding to a current density of ~114 mA/cm^2. The underlying phenomena explaining the trends shown in the figure are connected to the linear dependence of the OPEX on the cell voltage, which, for a given capacity, determines the total power input, and thus the total electricity demand (see Fig. 4b and Eq. (5)). For the CAPEX, on the other hand, the polarization curve shows an increase in the current density with the cell voltage (see *Supplementary Information*), as the overpotential applied raises – this means that for higher values of the voltage, smaller units are required for a given production capacity. The figure shows a dominating effect of the OPEX at higher voltages, but overall, the curve for the TAC is relatively flat above 3 V, providing flexibility and robustness to the electrolyzer design.

It should be remarked that the assumption of 1500 $/m^2 for the capital cost of the stacks is optimistic; however, for the design point considered (3.3 V, 114 mA/cm^2), this corresponds to 400 $/kW, which is consistent with cost projections for hydrogen electrolysis (IEA 2022). Higher capital costs for the electrolyzer would shift the optimum voltage to higher values, to reduce the size of the unit by driving up the current density: this would lead to even higher waste heat, thus strengthening the case for the heat pump solution.

The choice of the cell voltage determines also the amount of waste heat available for upgrading via the heat pump, according to Eq. (7). This effect is shown in Fig. 4b, which reports on the left y-axis both the total power input to the electrolyzers and the available waste heat as a function of the cell voltage, while the right y-axis shows the electrolysis cell energy efficiency. The latter is inversely proportional to the cell voltage (see Eq. (6)), demonstrating a loss of efficiency with higher voltages. These results highlight how the design of the electrolyzer has cascade effects on the performance of the rest of the process, as the electrolyzer efficiency could be improved, but this would increase the demand for external energy inputs for the downstream separation in the integrated system. With these conditions, the electrolyzers need to be supplied with a total electric power of ~31 MW_{el} and generate ~18

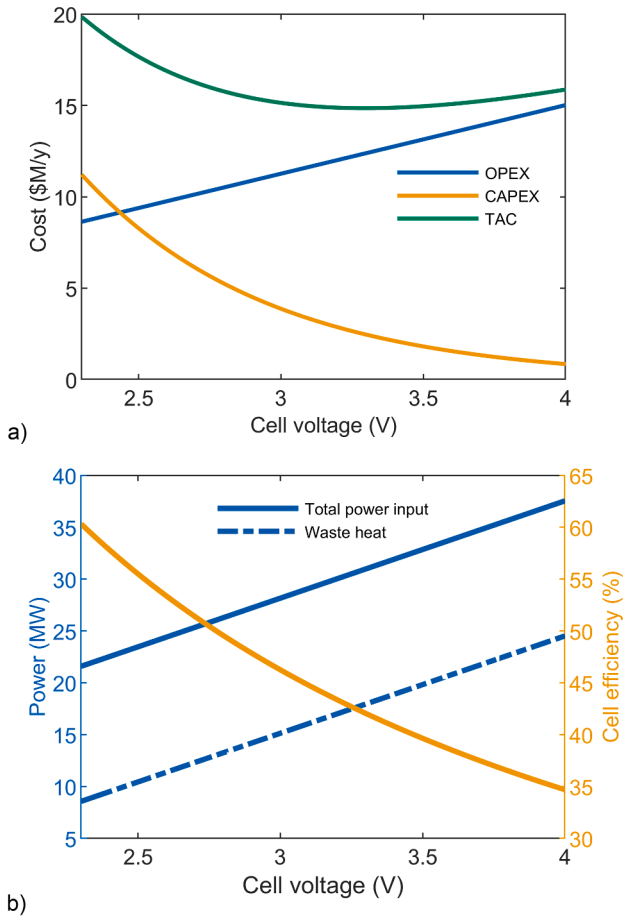

Fig. 4. Electrolyzer design. a) Trade-off between OPEX and CAPEX for the electrolyzer as a function of the cell voltage (electrolyzer lifetime: 5 years; electricity price: 0.05 $/kWh$_{el}$; electrolyzer cost: 1500 $/m^2); b) System trade-off showing the total power input to, and the waste heat developed by, the electrolyzers, as a function of the cell voltage. The cell efficiency vs. the voltage is also provided, under the same conditions.

MW_{th} of waste heat available at 50 °C, while operating at an energy efficiency of 42 %, as summarized in Table 1.

The total area for the electrolyzer amounts to 8240 m^2, which is five orders of magnitude larger than that of the largest currently operating CO_2 electrolyzers (e.g., a 10-cell stack with 800 cm^2 cells (Edwards et al. 2023), or to 1000 cm^2 plus 500 cm^2 tandem electrolyzer by Crandall, et al. (2024)). However, the technology is still in the early developmental stages, with only a few examples of pilot-scale plants (Belsa et al. 2024) and yet no industrial applications. Viewed in the light of industrial water electrolyzers, this area appears to be reasonable, as it is comparable with large installations for hydrogen production (e.g., 37, 500 m^2 reported by Smith et al. (2019)). In the future, with available data and/or additional validated mechanistic models at the relevant temperatures and scales, the model would benefit from the inclusion of their effects on kinetics, resistances, and overall cell performance. While this step would strengthen the generalizability of the results, the core insights into thermal integration remain valid within the current modelling framework

Table 1
Electrolyzer design variables and energy balance results.

Variable	Value	Unit of measure
Cell voltage	3.30	V
Current density	114	mA/cm^2
Formic acid Faradaic efficiency	66	%
Hydrogen Faradaic efficiency	31	%
Carbon monoxide Faradaic efficiency	3	%
Total power input	30.9	MW_{el}
Waste heat	17.9	MW_{th}
Energy efficiency	42	%
Total area needed	8240	m^2

3.2. Heat pump performance and energy integration

The performance of the heat pump is strongly influenced by the required temperature lift. In this work, the working fluid enters the evaporator at 35 °C, enabling the cooling of the anolyte (entering at 50 °C and exiting at 40 °C). The system is designed so that the working fluid reaches 120 °C at the condenser inlet, which is sufficient to supply the distillation column reboiler at 112 °C, as detailed in the following section. Although the required temperature lift of 67 °C is high (calculated based on the logarithmic mean temperatures of heat source and sink (Pieper et al. 2020)), it remains within current technology limits (Schlosser et al. 2020).

After screening different working fluids, we have identified HCFO-1233zd and ammonia as suitable candidates, due to their

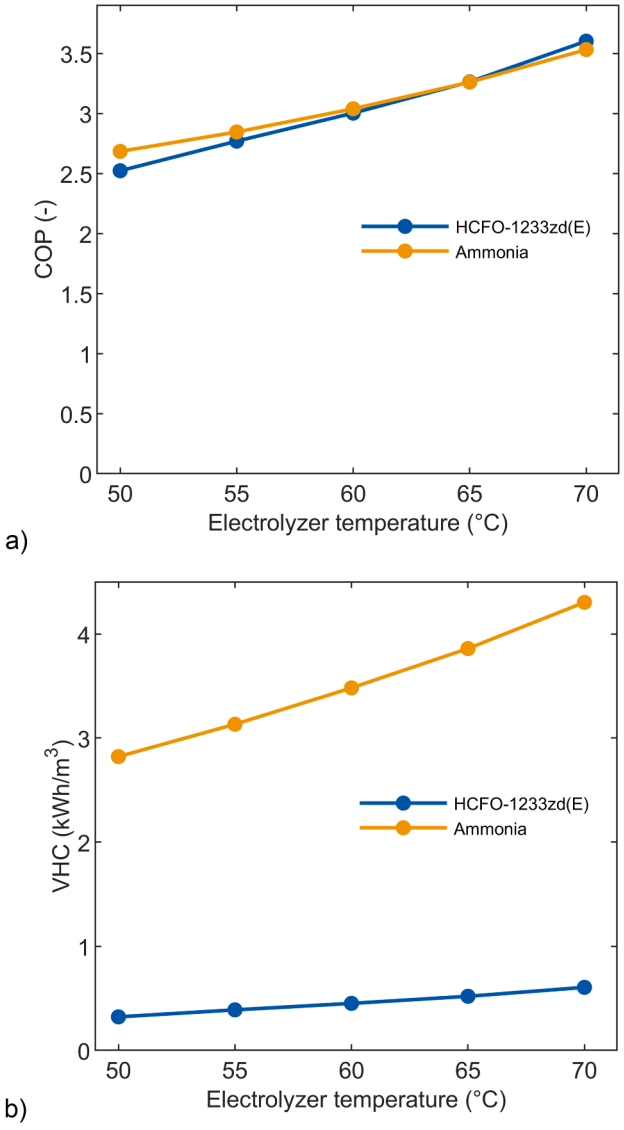

Fig. 5. Effect of the electrolyser operating temperature on heat pump performance. a) COP, b) VHC of the vapor compression heat pump, with two working fluids (HCFO-1233zd(E) and ammonia).

performance, appropriate critical temperature, and low global warming potential and ozone depletion potential (Arpagaus et al. 2018). The extended results of this screening, together with the details of the cycle operating conditions, are reported in the *Supplementary Information*. Based on the conditions, the heat pump can reach a COP of ~2.5–2.7, consistent with results for similar conditions reported in the literature (Van De Bor et al. 2015) and corresponding to a Lorenz efficiency of 44–47 %. The heat pump employs compressors requiring ~10.5–11.6 MW_{el} and delivers ~28–29 MW_{th} of upgraded heat at the target temperature: these values, albeit large, are aligned with high-temperature heat pumps technologies currently under industrial development (Zühlsdorf 2024). From the heat integration perspective, the two fluids lead to substantially similar results. However, the two differ significantly in the pressure levels required and have different flow rate requirements, with ammonia being much more efficient, having a VHC of 2.8 kWh/m^3, against only 0.32 kWh/m^3 for HCFO-1233zd.

Since the electrolyzer operating temperature is still subject to research, and possibly higher temperatures will be investigated as the technology progresses, the efficiency of the heat pump for the two working fluids selected is reported as a function of the electrolyzer working temperature in Fig. 5. Both the COP and the VHC increase with the temperature of the electrolyzer as the temperature lift is decreased: the COP increases by 32 and 43 % when operating at 70 °C instead of at 50 °C, for ammonia and HCFO-1233zd, respectively, while the VHC shows an even more marked increased, of 53 % and 88 % for the two fluids. These improvements translate into smaller, and thus less expensive, compressors (~7 MW_{el}), but at the compromise of reduced upgraded heat (see Eq. (10)). The consequences of these changes on the heat pump economics are presented in the *Supplementary Information*.

3.3. Full process

Fig. 6 shows the overall process flow diagram for the system. The reboiler heat duties for the azeotropic distillation and the vacuum

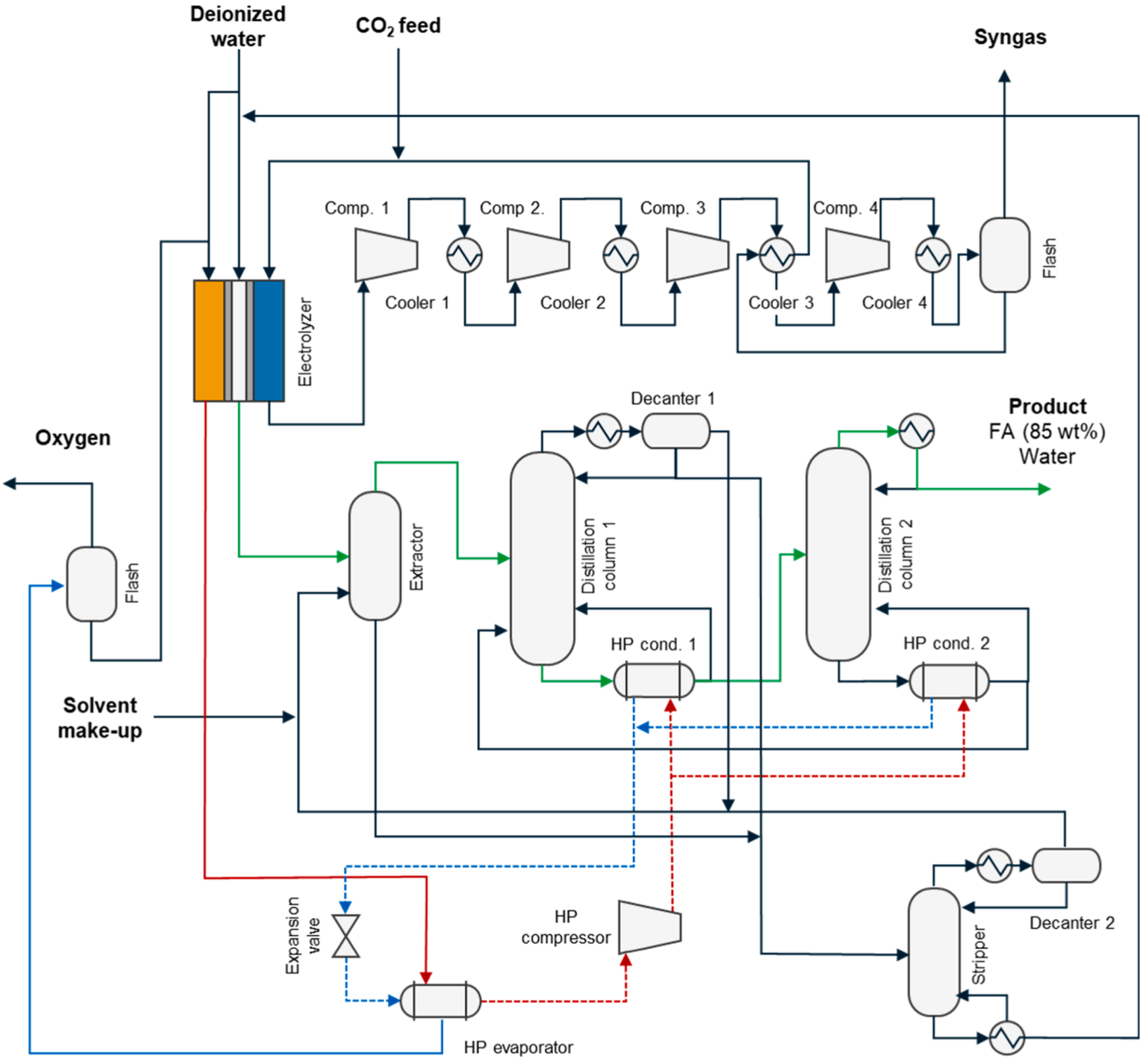

Fig. 6. Process Flow Diagram for the process. The main product path is highlighted in green, while red and blue represent hot and cold streams in the heat-integrated plant. The closed-circuit heat pump (HP) system is shown as a dashed line to distinguish it from the rest of the process.

Table 2
Main results of mass and energy balance, including key performance indicators.

Variable	Value	Units	Notes
Mass balance results			
Inlets			
CO_2	57	kt/y	N/A
Deionised water	36	kt/y	N/A
Solvent make-up	0.02	kt/y	N/A
Outlets			
Formic acid (85 wt %)	59	kt/y	N/A
Syngas (64 % H_2, 31 % CO_2, 4 % CO)	7.6	kt/y	N/A
Oxygen	26.7	kt/y	N/A
Energy balance results			
Distillation column 1 duty	25.5	MW_{th}	At 112 °C
Distillation column 2 duty	8.1	MW_{th}	At 92 °C
Stripper duty	3.8	MW_{th}	At 85 °C
CO_2 separation compression power (Comp. 1 to Comp. 4)	3.95	MW_{el}	N/A
CO_2 separation cooling requirements	0.6	MW	N/A
CO2 separation refrigeration	4.5	MW	N/A

distillation (Distillation columns 1 and 2, respectively, in Fig. 6) are 25 MW_{th} and 9 MW_{th}, respectively, while the stripper requires 3 MW_{th}. The reboilers operate at 112, 92, and 85 °C, respectively. Table 2 reports the main results of the mass and energy balances, including calculated Key Performance Indicators. The syngas obtained is a mixture of 65 mol % H_2, 31 mol % unconverted CO_2, and 4 mol % CO, which is compressed at 40 bar. This stream has a high carbon content (stoichiometric number of ~1, based on the definition provided in Kiss et al. (2016)), meaning that for utilization it would require enrichment with extra hydrogen: this has been accounted for in the price of the syngas considered for the economic analysis.

The overall system requires energy inputs of both electric and thermal nature. Since the former can be readily supplied by renewable means, while the latter is mostly derived from fossil fuels, it is of interest to look at both the overall energy demand of the process and then to compare the separate contributions of the electric and the thermal energy. Fig. 7 summarizes the main energy flows among the three sections of the system: the upgraded heat covers 76 % of the thermal energy requirements of the downstream, leaving only 24 % to be supplied by external heat. The heat pump thus accomplishes the dual goal of providing cooling to the electrolyzer system and delivering high temperature heat to the separation. Overall, electricity constitutes ~84 % of the energy inputs to the process. The analogous figure for the case without the heat pump is reported in the *Supplementary Information*, showing that electricity is 49 % of the total energy supply, with the remaining half being thermal energy.

The operation at lower cell efficiencies determines the availability of a sufficient amount of waste heat to cover the vast majority of the downstream duties, after upgrading with the heat pump. Thus, the energy integration system proposed unlocks efficient overall process performance even with the sacrifice of a locally optimal operation for the electrolyzer. In the base case (no heat pump), the thermal energy input is higher and the electrical energy input is lower, while in the heat pump case the energy inputs are reversed.

It should be noted that the proposed heat integration, considering the tight temperature approach margins, would pose control challenges at the industrial level, and the effects of cell efficiency decreases due to performance degradation (Van Der Roest et al. 2023) and of possible dynamic operation of the electrolyzers to follow a variable electricity input are still unexplored in this context. Other heat pump technologies, such as compression-resorption heat pumps (Van De Bor et al. 2014), could be explored as alternatives to the single-fluid vapor compression heat pumps.

3.4. Economic and environmental assessment

The economics of the process are evaluated in two different scenarios, with and without the heat pump. Fig. 8a and Fig. 8b shows the results of the economic evaluation in terms of annualized CAPEX and OPEX. The heat pump has a significant impact on the CAPEX, as it accounts for an increase of the total installed cost of 22 % compared to the case without it. The electrolyzer stacks are the most expensive units in the process, and, with a lifetime of 5 years implying four unit installations during the plant lifetime, they account for 46 % of the CAPEX in the scenario with the heat pump, and 56 % in the one without. The electrolyzer also represents the dominant contribution to the OPEX, accounting for >50 % of the operating expenses in either case. The lower OPEX associated with the heat pump scenario highlights the multiplying effect of the COP, by which the reduction in primary energy demand leads to lower total utilities costs, despite the higher cost of electricity compared to thermal energy.

Fig. 8c shows the results of the sensitivity analysis on the levelized production cost of formic acid, based on ±30 % variations in the inputs. The biggest drivers in the economic performance of the process are the electricity cost, which shifts the production cost by ±11 %, and the electrolyzer lifetime, which can increase the total CAPEX by 11 % when its reduced from 5 to 3 years (thus requiring 7 installations over the plant lifetime), while an increase in the lifetime to 7 years only reduces

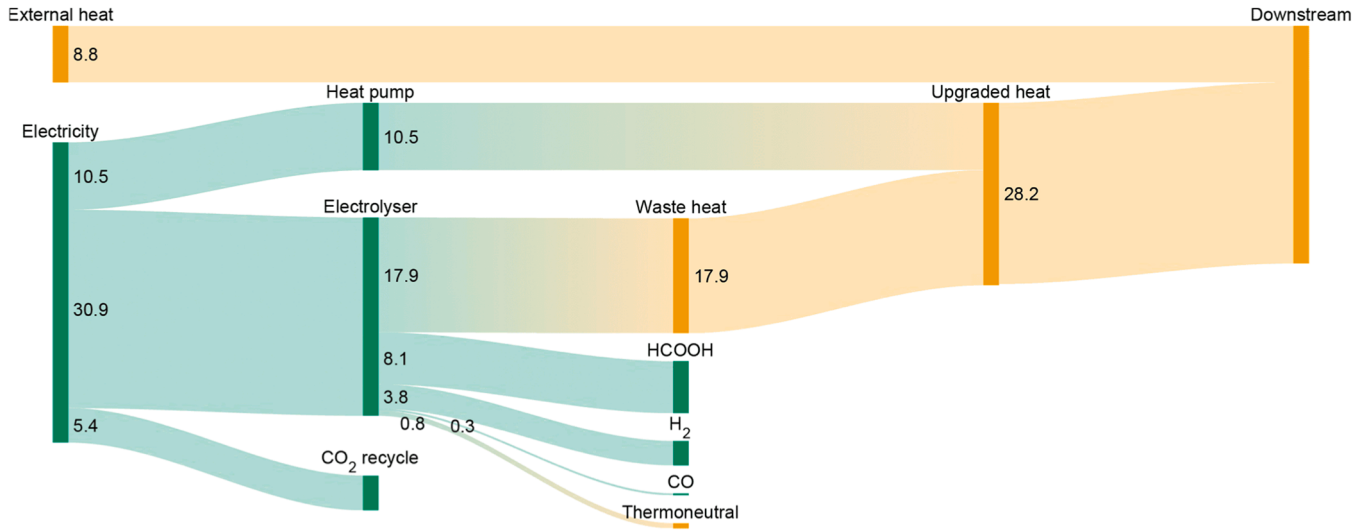

Fig. 7. Sankey diagram displaying the energy flows (in MW) in the system. Electric energy is shown as green, while thermal energy is represented in orange.

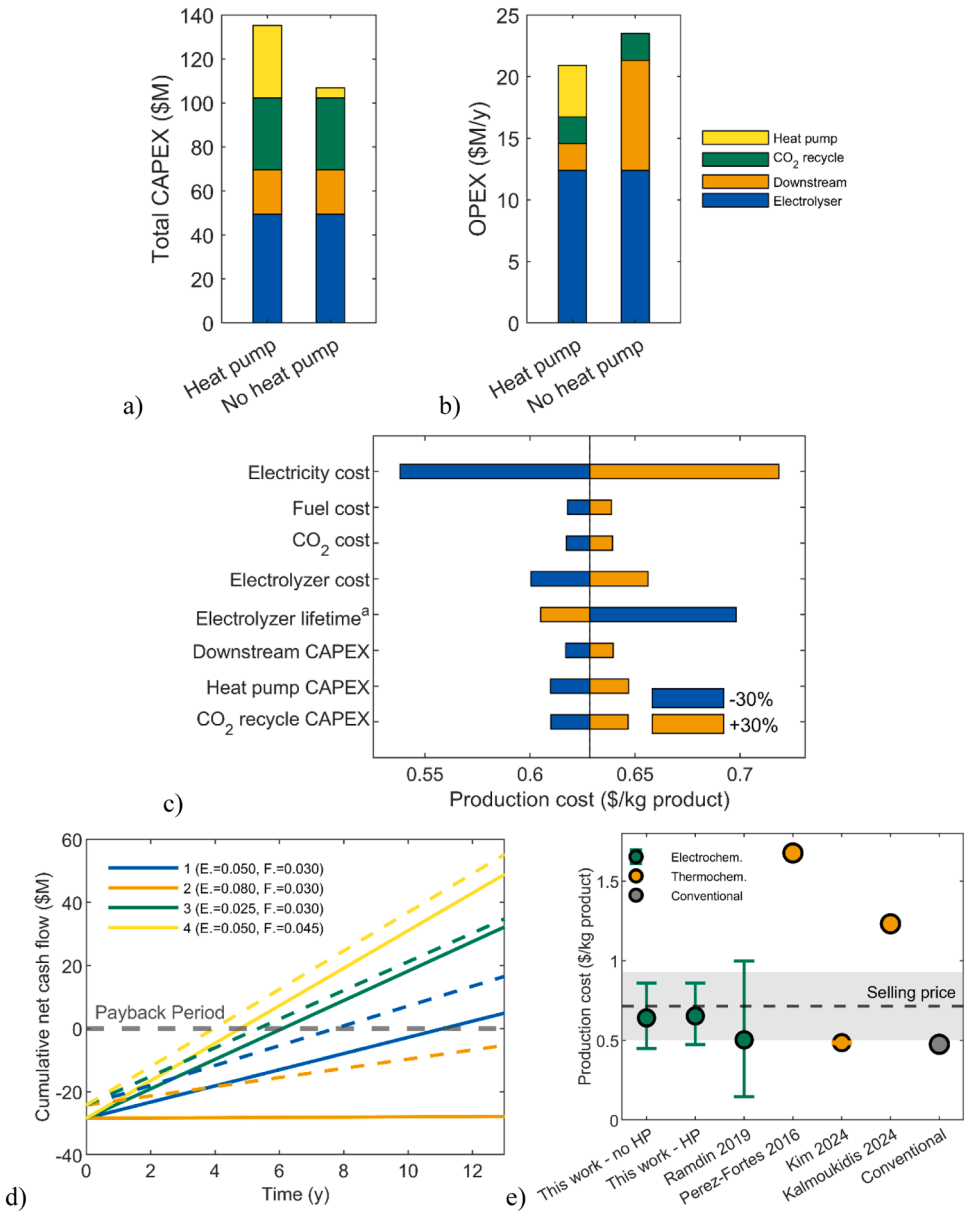

Fig. 8. Economic assessments of the scenarios with and without the heat pump. Panels a) and b) show the total CAPEX and OPEX for the plant for the scenarios with and without the heat pump. The CAPEX is the total over the lifetime of the plant, thus including multiple electrolyzer replacements. Panel c) reports the results of the sensitivity analysis on the levelized production cost for the heat pump scenario, with respect to the most important parameters (superscript a for the electrolyzer lifetime indicates changes different from ±30 %). Panel d) represents the cumulative net cash flow for the investment in the heat pump, showing different scenarios based on the electricity (E.) and fuel (F.) price (reported in $/kWh$_{el}$ and $/kWh$_{th}$, respectively); solid lines are for electrolyzer operating at 50 °C, while dashed lines are for operation at 70 °C. Panel e) compares the levelized production cost obtained in this work with results found in the literature for other productions of formic acid (electrochemical, thermochemical, and conventional).

the CAPEX by 4 %, results which are consistent with the literature (Spurgeon and Kumar 2018). Notably, the electrolyzer cost has a significant, but moderate effect (4 %); however, radical differences in electrolyzer cost (e.g., due to the persistent use of rare elements like iridium) would have more significant impacts on the plant economics.

The heat pump is not an integral part of the process; thus, it could be regarded as an additional investment for which we can evaluate the payback period. The results are displayed in Fig. 8d for different scenarios of electricity and fuel prices, with the base case represented with solid lines (electrolyzer operating temperature 50 °C). The figure shows that the investment is paid back in less than ~11 years in the base case (0.05 $/kWh$_{el}$, 0.03 $/kWh$_{th}$), and is more advantageous in the cases in which electricity has a very low cost (0.025 $/kWh$_{el}$) or fuel is more expensive (0.045 $/kWh$_{th}$). However, higher electricity prices, corresponding to current values (0.08 $/kWh$_{el}$ (U.S. Energy Information Administration, 2025)), make this design economically unattractive. Furthermore, it can be observed that the system is sensitive to increases in the fuel prices, given that the payback period for scenario 4 (electricity price of 0.05 $/kWh$_{el}$ and fuel price of 0.045 $/kWh$_{th}$) is less than half (5 years) of that for scenario 1 (same electricity price, 0.03 $/kWh$_{th}$ for fuel). The figure also shows the results for the case of higher operating temperature (70 °C), reported as dashed lines. Requiring a smaller compressor due to the higher COP, the total investment is reduced by ~15 % (reflected in the less negative value at time zero) and leading to a payback period 30 % shorter in the base case price scenario, and 12–17 % shorter for price scenarios 3 and 4. The more efficient heat pump has a shorter payback period than the plant lifetime (17 compared to 20 years), even in the high electricity cost scenario 2.

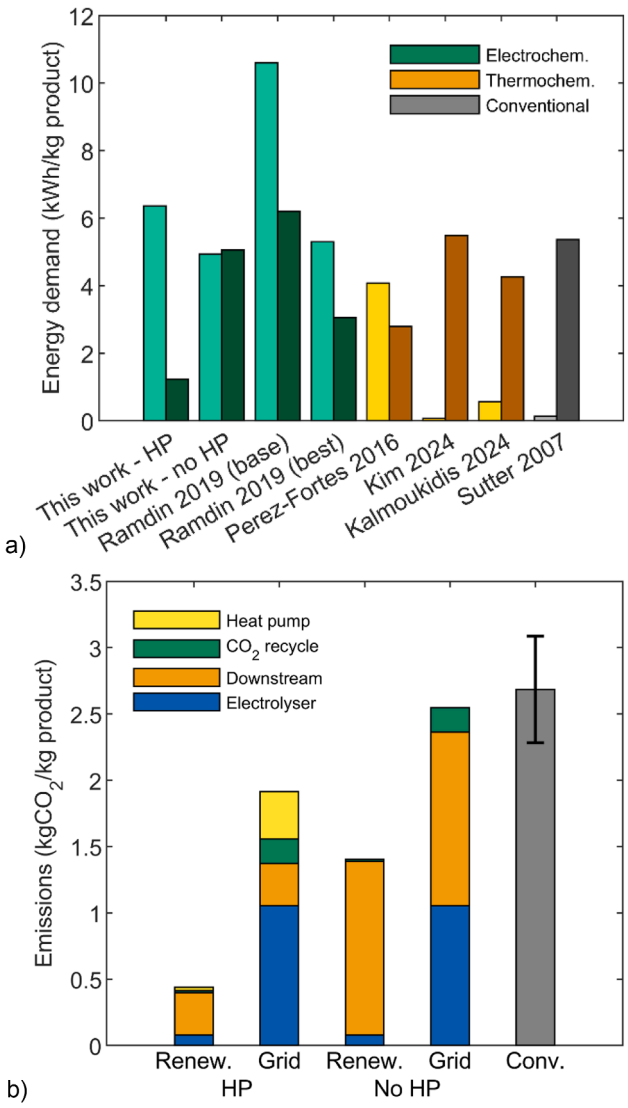

Fig. 9. Energy demand and carbon dioxide emissions per unit product, with and without heat pump (HP and no HP, respectively). Panel a) differentiates between electricity (lighter shade) and thermal energy (darker shade) inputs. Panel b) includes scenarios with different electricity sources (grid, renewables) and the emissions of the conventional (Conv., fossil-based) production of formic acid.

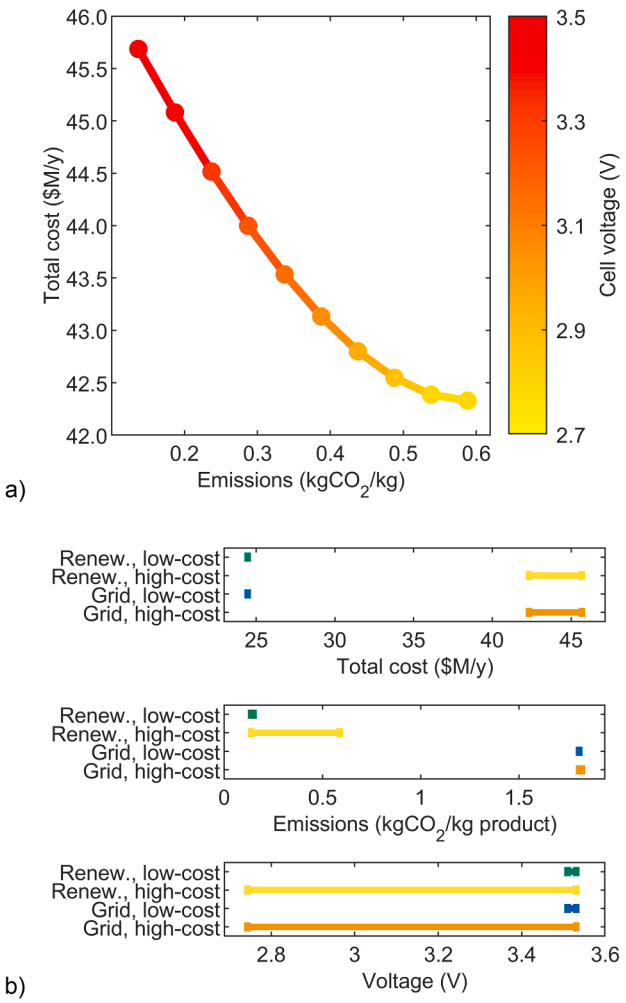

Fig. 10. Results of the optimization. a) Pareto front for the multi-objective optimization (total cost vs. CO_2 emissions per unit product), with renewable (19 gCO_2/kWh), high-cost electricity (0.1 \$/kWh_{el}). b) Ranges for the objective functions and the decision variable for the 4 scenarios. Note that the total cost excludes the downstream separation and CO_2 recovery.

Fig. 8e presents a comparison of the results of several techno-economic assessments for formic acid production from carbon dioxide, including the conventional production as a benchmark and reporting the selling price of the product (assumed to vary in $a \pm 30$ % range). The error bars reported account for the variables reported in the sensitivity analysis being all at their most or least favorable values. This shows how the process developed, together with the techno-economic assumptions made based on literature cost projections, would be profitable only with a high product selling price and cannot yet compete with conventional productions or with the state-of-the-art thermochemical process, demonstrated at the pilot scale (Kim et al. 2024). However, the marked electrification of our design could prove advantageous in future scenarios with declining electricity prices (Mills et al. 2021) and/or penalties being imposed on carbon emissions (Mengesha and Roy 2025).

The energy demand per unit product can be seen in Fig. 9a, where the electrical and thermal contributions are separated, with the former represented by a lighter shade and the latter by a darker one. The difference in total energy demand can be attributed to the multiplying effect of the coefficient of performance of the heat pump. As demonstrated by Fig. 7 and its counterpart in the *Supplementary Information* for the scenario without the heat pump, a higher total primary energy input is required when providing heat through an external source (e.g. steam boiler): on top of the economic benefits discussed, the process configuration including the heat pump is beneficial from the perspective of primary energy demand, considered a limited resource. The thermal energy demand is comparable, even in the case without the heat pump, to that of the thermochemical processes, for which, it should be noted, electrolytic hydrogen production is considered outside battery limits (except for (Pérez-Fortes et al. 2016), hence the higher electricity demand).

Fig. 9b reports the emissions per unit product allocated to the different sections of the process, adding to the analyses the cases in which the electricity is sourced from renewables (based on offshore wind (U.S. Department of Energy 2015)) and from a grey grid (average EU (European Environment Agency, 2025)). The application of renewables to the process leads to a significant reduction in emissions compared to the conventional, fossil-based production, even without the heat pump. However, due to the large electricity demand of the electrolyzer, powering it with grey electricity would result in significant emissions, comparable to those of the conventional production. In the case of renewables usage, the heat pump contributes to a reduction of CO_2 emissions by 84 %, while the carbon footprint advantages of using

the heat pump when the compressor exploits grey electricity are reduced to only 29 %. Comparing the scenarios with and without the heat pump, the heat pump leads to a relative reduction of 25–69 % of the scope 2 emission, with grid and renewables, respectively.

3.5. Optimization

The optimization for the total cost (for electrolyzer and heat pump) and carbon dioxide emissions is run in different scenarios, depending on the price and source of electricity (fully renewable or grid). The results are displayed in Fig. 10a, which shows the Pareto front for the case of high cost renewable electricity (0.1 $/kWh, 19 gCO_2/kWh), together with the value of the cell voltage with yields the optimal conditions. For this case, the points with lower cost display relatively small variations (~7 %), showing a flatter profile, while the emissions show a larger change (from 0.14 to 0.59 $kgCO_2$/kg product). The trade-off between these two variables appears clearly as high voltages (~3.5 V) lead to lower emissions but overall higher costs, when a large heat pump is used to cover the full separation energy demand, while lower voltages (2.7–2.8 V) minimize the costs but compromise the emission reduction in the process. Given the modest increase in total cost brought by operating at higher voltages, compared to the greater environmental benefit, the operation at 3.5 V should be preferred. It should be noted that the figure reports total costs as a combination of annualized CAPEX and OPEX for the system composed of electrolyzer, heat pump, and heat exchangers involved in the energy-integrated system.

Fig. 10b compares the results for the objective functions and the decision variables for the four scenarios considered. The figure emphasizes the different ranges that the input and outputs show in the different scenarios, highlighting that with low-cost electricity, the solution is trivial regardless of the electricity source, and always operates at high voltage (~3.5 V). This operation minimizes the cost, while the emissions do not play a big role in pushing for different results, as they are either low (with renewables) or high (with grid). With high-cost grid electricity, the emissions are always high, thus the minimum voltage is preferred as it reduces the cost. We demonstrate that our methodology can be successfully applied to decide the value of the cell voltage for process optimization. This can be further extended by including other decision variables depending on the design needs. Examples of possible decision variables are: input flow rates to the electrolyzer; electrolyzer operating temperature, conditional on the availability of experimental data; heat pump pressure levels and approach temperatures.

4. Conclusions

This work addressed two issues presented by low temperature carbon dioxide electrolysis processes to liquid products, namely waste heat management and separation of diluted product streams. Alongside this, we have filled a gap with respect to the lack of studies developing process-level understanding of the trade-offs present in these systems.

Coupling the electrolyzer waste heat with the downstream energy demand via a mechanically-driven heat pump, we have demonstrated an effective way to reduce external energy inputs, furthering the penetration of electricity in the process, up to 76 % of the total energy inputs. This leads to carbon dioxide emissions reduced by 84 % (with renewables) or by 29 % (with grid electricity) with respect to the conventional production, showing that lower emissions are achievable even considering the diluted nature of the electrolyzer outlet. Additionally, the economic performance of the heat pump would justify the increased capital investment, with an investment recouped in 11 years for the base case, but in 5–6 years in the case of cheaper electricity or more expensive fuel.

Furthermore, our analysis of the heat pump performance with respect to the electrolyzer operating temperature shows that a 20 °C increase in this variable (from 50 to 70 °C) can lead to significant improvements in the COP (from 2.5–2.7 to 3.5–3.6) and VHC (0.3 to 0.6 kWh/m^3 for HCFO-1233zd(E), and 2.8 to 4.3 kWh/m^3 for ammonia), improvements which make the business case for the heat pump more compelling, while simultaneously reducing emissions further.

The optimization of the process provides insights into the trade-offs for the energy integrated plant, showing how, under different circumstances of power supply, the optimal operating conditions can be found by either pushing the cell voltage to get enough waste heat to cover all the downstream demand (3.5 V), or either at lower voltages to reduce total cost. With more detailed electrolyzer models and with increasing emphasis on the operating temperature of the electrolyzer, it will be possible to extend the process optimization to account for multiple decision variables and let it encompass the operating temperature itself, to guide experimental efforts as well as techno-economic ones. At the same time, other heat pump technologies can be researched, e.g., compression-resorption heat pumps, which could have higher coefficients of performance, while including the cycle operating conditions (pressures, approach temperatures) among the decision variables. This will lead to globally more efficient processes, even if this comes at a compromise of the locally optimal energetic performance of the electrolyzer.

Our work highlights the importance of system-wide process integration and analysis to unlock more sustainable process designs for electrochemical reduction of carbon dioxide, with implications for both the research and the industrial communities.

CRediT authorship contribution statement

Riccardo Dal Mas: Writing – review & editing, Writing – original draft, Visualization, Validation, Supervision, Software, Methodology, Investigation, Formal analysis, Data curation, Conceptualization. **Andrea Carta:** Visualization, Software, Methodology, Investigation, Formal analysis. **Ana Somoza-Tornos:** Writing – review & editing, Supervision, Methodology. **Anton A. Kiss:** Writing – review & editing, Writing – original draft, Validation, Supervision, Methodology, Formal analysis, Conceptualization.

Declaration of competing interest

The authors declare that they have no known competing financial interests or personal relationships that could have appeared to influence the work reported in this paper.

Supplementary materials

Supplementary material associated with this article can be found, in the online version, at doi:10.1016/j.compchemeng.2025.109330.

Data availability

Data is available in the supplementary material.

References

Alerte, Théo, Gaona, Adriana, Edwards, Jonathan P., et al., 2023. Scale-dependent techno-economic analysis of CO $_2$ capture and electroreduction to ethylene. ACS Sustain. Chem. Eng. 11 (43), 15651–15662. https://doi.org/10.1021/acssuschemeng.3c04373.

Arpagaus, Cordin, Bless, Frédéric, Uhlmann, Michael, Schiffmann, Jürg, Bertsch, Stefan S., 2018. High temperature heat pumps: market overview, State of the art, research status, refrigerants, and application potentials. Energy 152, 985–1010. https://doi.org/10.1016/j.energy.2018.03.166. June.

Aspen Technology, Inc. 2013. "Aspen physical property System." November. https://www.aspentech.com.

Bains, Praveen, Psarras, Peter, Wilcox, Jennifer, 2017. CO 2 capture from the industry sector. Prog Energy Combust. Sci. 63, 146–172. https://doi.org/10.1016/j.pecs.2017.07.001. November.

Bangalore Ashok, Prasad Rahul, Oinas, Pekka, Forssell, Susanna, 2022. Techno-economic evaluation of a biorefinery to produce γ-valerolactone (GVL), 2-methyltetrahydrofuran (2-MTHF) and 5-hydroxymethylfurfural (5-HMF) from Spruce. Renew. Energy. 190, 396–407 May doi:10.1016/j.renene.2022.03.128.

Barecka, Magda H., Dameni, Pritika Ds, Muhamad, Marsha Zakir, Ager, Joel W., Lapkin, Alexei A., 2023. Energy-efficient ethanol concentration method for scalable CO_2 electrolysis. ACS Energy Lett. 8 (7), 3214–3220. https://doi.org/10.1021/acsenergylett.3c00973.

Bauer, Fredric, Tilsted, Joachim P, Pfister, Stephan, Oberschelp, Christopher, Kulionis, Viktoras, 2023. Mapping GHG emissions and prospects for renewable energy in the chemical industry. Curr. Opin. Chem. Eng. 39, 100881. https://doi.org/10.1016/j.coche.2022.100881. March.

Belsa, Blanca, Xia, Lu, Pelayo García De Arquer, F., 2024. CO_2 Electrolysis Technologies: bridging the gap toward scale-up and commercialization. ACS Energy Lett. 9 (9), 4293–4305. https://doi.org/10.1021/acsenergylett.4c00955.

Berkelaar, Lotte, Van Der Linde, Joram, Peper, Julia, et al., 2022. Electrochemical conversion of carbon dioxide to ethylene: plant design, evaluation and prospects for the future. Chemic. Eng. Res. Des. 182, 194–206. https://doi.org/10.1016/j.cherd.2022.03.034. June.

Bonanno, Marco, Müller, Karsten, Bensmann, Boris, et al., 2024. Review and prospects of PEM water electrolysis at elevated temperature operation. Adv. Mater. Technol. 9 (2), 2300281. https://doi.org/10.1002/admt.202300281.

Chatterjee, Sudipta, Dutta, Indranil, Lum, Yanwei, Lai, Zhiping, Huang, Kuo-Wei, 2021. Enabling storage and utilization of low-carbon electricity: power to formic acid. Energy Environ. Sci. 14 (3), 1194–1246. https://doi.org/10.1039/D0EE03011B.

Chua, W.X., Cunha, S.Da, Rangaiah, G.P., Hidajat, K., 2019. Design and optimization of Kemira-Leonard process for formic acid production. Chemic. Eng. Sci. 2, 100021. https://doi.org/10.1016/j.cesx.2019.100021. May.

Crandall, Bradie S., Brix, Todd, Weber, Robert S., Jiao, Feng, 2023. Techno-economic assessment of green H_2 carrier supply chains. Energy Fuel. 37 (2), 1441–1450. https://doi.org/10.1021/acs.energyfuels.2c03616.

Crandall, B.S., Ko, B.H., Overa, S., Cherniack, L., Lee, A., Minnie, I., Jiao, F., 2024. Kilowatt-scale tandem CO2 electrolysis for enhanced acetate and ethylene production. Nat. Chemic. Eng. 1, 421–429.

Da Cunha, Sergio, Rangaiah, G.P., Hidajat, Kus, 2018. Design, optimization, and retrofit of the Formic acid process I: base case Design and dividing-wall column retrofit. Ind. Eng. Chem. Res. 57 (29), 9554–9570. https://doi.org/10.1021/acs.iecr.8b00883.

De Luna, Phil, Hahn, Christopher, Higgins, Drew, Jaffer, Shaffiq A., Jaramillo, Thomas F., Sargent, Edward H., 2019. What would it take for renewably powered electrosynthesis to displace petrochemical processes? Science 364 (6438), eaav3506. https://doi.org/10.1126/science.aav3506.

Dioxide Materials. (2024, 07 24). *CO2 Conversion to formic acid*. Retrieved from Dioxide Materials: https://dioxidematerials.com/technology/formic-acid/.

Eckl, Florentin, Moita, Ana, Castro, Rui, Neto, Rui Costa, 2025. Valorization of the by-product oxygen from green hydrogen production: a review. Appl. Energy 378, 124817. https://doi.org/10.1016/j.apenergy.2024.124817. January.

Edwards, Jonathan P., Alerte, Théo, O'Brien, Colin P., et al., 2023. Pilot-scale CO_2 electrolysis enables a semi-empirical electrolyzer model. ACS Energy Lett. 8 (6), 2576–2584. https://doi.org/10.1021/acsenergylett.3c00620.

European Environment Agency. (2025, 03 05). *Greenhouse gas emission intensity of electricity generation in Europe*. Retrieved from European Environment Agency: https://www.eea.europa.eu/en/analysis/indicators/greenhouse-gas-emission-intensity-of-1?activeAccordion=.

Fernández-Caso, Kevin, Díaz-Sainz, Guillermo, Alvarez-Guerra, Manuel, Irabien, Angel, 2023. Electroreduction of CO_2: advances in the continuous production of formic acid and formate. ACS Energy Lett. 8 (4), 1992–2024. https://doi.org/10.1021/acsenergylett.3c00489.

Frate, Guido Francesco, Ferrari, Lorenzo, Desideri, Umberto, 2019. Analysis of suitability ranges of high temperature heat pump working fluids. Appl. Therm. Eng. 150, 628–640. https://doi.org/10.1016/j.applthermaleng.2019.01.034. March.

Gabardo, Christine M., O'Brien, Colin P., Edwards, Jonathan P., et al., 2019. Continuous carbon dioxide electroreduction to concentrated multi-carbon products using a membrane electrode assembly. Joule 3 (11), 2777–2791. https://doi.org/10.1016/j.joule.2019.07.021.

Galvan-Cara, Aldwin-Lois, Bongartz, Dominik, 2025. Rethinking electrolyzer design for optimal waste-heat utilization. Appl. Energy. 398, 126367. https://doi.org/10.1016/j.apenergy.2025.126367. November.

Ge, Xiaolong, Zhang, Ran, Liu, Pengfei, Liu, Botan, Liu, Botong, 2023. Optimization and control of extractive distillation for formic acid-water separation with maximum-boiling azeotrope. Comput. Chem. Eng. 169, 108075. https://doi.org/10.1016/j.compchemeng.2022.108075. January.

Goldman, Maxwell, Prajapati, Aditya, Duoss, Eric, Baker, Sarah, Hahn, Christopher, 2023. Bridging fundamental science and applied science to accelerate CO2 electrolyzer scale-up. Curr. Opinion Electrochem. 39, 101248. https://doi.org/10.1016/j.coelec.2023.101248. June.

Harrison, K.W., Remick, R., Martin, G.D., Hoskin, A., 2010. Hydrogen production: fundamentals and case study summaries. In: Paper presented at 18th World Hydrogen Energy Conference, Essen, Germany.

Hietala, Jukka, Vuori, Antti, Johnsson, Pekka, Pollari, Ilkka, Reutemann, Werner, Kieczka, Heinz, 2016. Formic acid. Ullmann's Encyclopedia of Industrial Chemistry, 1st ed. Wiley-VCH. Wiley. https://doi.org/10.1002/14356007.a12_013.pub3. edited by.

Hu, Leiming, Wrubel, Jacob A., Baez-Cotto, Carlos M., et al., 2023. A scalable membrane electrode assembly architecture for efficient electrochemical conversion of CO2 to formic acid. Nat. Commun. 14 (1), 7605. https://doi.org/10.1038/s41467-023-43409-6.

Huber, Marcia L., Lemmon, Eric W., Bell, Ian H., McLinden, Mark O., 2022. The NIST REFPROP Database for highly accurate properties of industrially important fluids. Ind. Eng. Chem. Res. 61 (42), 15449–15472. https://doi.org/10.1021/acs.iecr.2c01427.

Huijbregts, Mark A.J., Steinmann, Zoran J.N., Elshout, Pieter M.F., et al., 2017. ReCiPe2016: a harmonised life cycle impact assessment method at midpoint and endpoint level. Int. J. Life Cycle Assess. 22 (2), 138–147. https://doi.org/10.1007/s11367-016-1246-y.

Hurkmans, Jan-Willem, Pelzer, Henri M., Burdyny, Tom, Peeters, Jurriaan, Vermaas, David A., 2025. Heating dictates the scalability of CO_2 electrolyzer types. EES Catal. https://doi.org/10.1039/D4EY00190G.

IEA. 2022. *Global Hydrogen Review 2022*. Paris.

IEA. 2024. *Renewables 2024.Pdf*. Paris. https://www.iea.org/reports/renewables-2024.

Jiang, Jiatong, Hu, Bin, Wang, R.Z., Deng, Na, Cao, Feng, Wang, Chi-Chuan, 2022. A review and perspective on industry high-temperature heat pumps. Renew. Sustain. Energy Rev. 161, 112106. https://doi.org/10.1016/j.rser.2022.112106. June.

Kalmoukidis, Nikolaos, Barus, Amsalia, Staikos, Savvas, Taube, Maximiliano, Mousazadeh, Farzad, Kiss, Anton A., 2024. Novel process design for eco-efficient production of green formic acid from CO2. Chemic. Eng. Res. Des. 210, 425–436. https://doi.org/10.1016/j.cherd.2024.09.001. October.

Kato, Takeyoshi, Kubota, Mitsuhiro, Kobayashi, Noriyuki, Suzuoki, Yasuo, 2005. Effective utilization of by-product oxygen from electrolysis hydrogen production. Energy 30 (14), 2580–2595. https://doi.org/10.1016/j.energy.2004.07.004.

Kibria, Md Golam, Edwards, Jonathan P., Gabardo, Christine M., et al., 2019. Electrochemical CO_2 reduction into chemical feedstocks: from mechanistic electrocatalysis models to system design. Advanc. Mater. 31 (31), 1807166. https://doi.org/10.1002/adma.201807166.

Kibria Nabil, Shariful, McCoy, Sean, Kibria, Md Golam, 2021. Comparative life cycle assessment of electrochemical upgrading of CO_2 to fuels and feedstocks. Green Chem. 23 (2), 867–880. https://doi.org/10.1039/D0GC02831B.

Kim, Changsoo, Park, Kwangho, Lee, Hyeonggeon, et al., 2024. Accelerating the net-zero economy with CO2-hydrogenated formic acid production: process development and pilot plant demonstration. Joule 8 (3), 693–713. https://doi.org/10.1016/j.joule.2024.01.003.

Kiss, Anton A., Infante Ferreira, Carlos A., 2016. Heat Pumps in Chemical Process Industry, 1st ed. CRC Press. https://doi.org/10.1201/9781315371030.

Kiss, Anton A., Smith, Robin, 2020. Rethinking energy use in distillation processes for a more sustainable chemical industry. Energy 203, 117788. https://doi.org/10.1016/j.energy.2020.117788. July.

Kiss, Anton A., Pragt, J.J., Vos, H.J., Bargeman, G., De Groot, M.T., 2016. Novel efficient process for methanol synthesis by CO 2 hydrogenation. Chemic. Eng. J. 284, 260–269. https://doi.org/10.1016/j.cej.2015.08.101. January.

Kraft, Dieter. 1988. *A software package for Sequential quadratic programming*. DFVLR-FB 88-28. Deutsche Forschungs- und Versuchsanstalt für Luftund Raumfahrt.

Lee, Wonhee, Kim, Young Eun, Hye Youn, Min, Jeong, Soon Kwan, Park, Ki Tae, 2018. Catholyte-free electrocatalytic CO_2 reduction to formate. Angewandte Chemie. Int. Edit. 57 (23), 6883–6887. https://doi.org/10.1002/anie.201803501.

Lemmon, E.W., Bell, I.H., Huber, M.L., & McLinden, M.O. (2018). *NIST Standard Reference Database 23: reference Fluid Thermodynamic and Transport Properties-REFPROP, version 10.0, National Institute of Standards and Technology*. doi:https://doi.org/10.18434/T4/1502528.

Luyben, William L., 2018. Capital cost of compressors for conceptual design. Chemic. Eng. Process. - Proc. Intensificat. 126, 206–209. https://doi.org/10.1016/j.cep.2018.01.020. April.

Madeddu, Silvia, Ueckerdt, Falko, Pehl, Michaja, et al., 2020. The CO_2 reduction potential for the European industry via direct electrification of heat supply (Power-to-Heat). Environment. Res. Lett. 15 (12), 124004. https://doi.org/10.1088/1748-9326/abbd02.

Mahida, Badra, Benyounes, Hassiba, Shen, Weifeng, 2021. Process analysis of pressure-swing distillation for the separation of formic acid–Water mixture. Chemic. Paper. 75 (2), 599–609. https://doi.org/10.1007/s11696-020-01329-5.

Mallapragada, Dharik S., Dvorkin, Yury, Modestino, Miguel A., et al., 2023. Decarbonization of the chemical industry through electrification: barriers and opportunities. Joule 7 (1), 23–41. https://doi.org/10.1016/j.joule.2022.12.008.

Martín, Antonio J., Larrazábal, Gastón O., Pérez-Ramírez, Javier, 2015. Towards sustainable fuels and chemicals through the electrochemical reduction of CO_2: lessons from water electrolysis. Green Chem. 17 (12), 5114–5130. https://doi.org/10.1039/C5GC01893E.

Masel, Richard I., Liu, Zengcai, Yang, Hongzhou, et al., 2021. An industrial perspective on catalysts for low-temperature CO2 electrolysis. Nat. Nanotechnol. 16 (2), 118–128. https://doi.org/10.1038/s41565-020-00823-x.

Mavrotas, George., 2009. Effective implementation of the ε-constraint method in multi-objective mathematical programming problems. Appl. Math. Comput. 213 (2), 455–465. https://doi.org/10.1016/j.amc.2009.03.037.

Mengesha, Isaak, Roy, Debraj, 2025. Carbon pricing drives critical transition to green growth. Nat. Commun. 16 (1). https://doi.org/10.1038/s41467-025-56540-3.

Mills, Andrew, Wiser, Ryan, Millstein, Dev, et al., 2021. The impact of wind, solar, and other factors on the decline in wholesale power prices in the United States. Appl. Energy. 283, 116266. https://doi.org/10.1016/j.apenergy.2020.116266. February.

O'Brien, Colin P., Miao, Rui Kai, Zeraati, Ali Shayesteh, Lee, Geonhui, Sargent, Edward H., Sinton, David, 2024. CO_2 electrolyzers. Chem. Rev. 124 (7), 3648–3693. https://doi.org/10.1021/acs.chemrev.3c00206.

Orella, Michael J., Brown, Steven M., Leonard, McLain E., Román-Leshkov, Yuriy, Brushett, Fikile R., 2020. A general technoeconomic model for evaluating emerging electrolytic processes. Energy Technol. 8 (11), 1900994. https://doi.org/10.1002/ente.201900994.

Pérez-Fortes, Mar, Schöneberger, Jan C., Boulamanti, Aikaterini, Harrison, Gillian, Tzimas, Evangelos, 2016. Formic acid synthesis using CO2 as raw material: techno-economic and environmental evaluation and market potential. Int. J. Hydrogen Energy. 41 (37), 16444–16462. https://doi.org/10.1016/j.ijhydene.2016.05.199.

Pace, Vittorio, Hoyos, Pilar, Castoldi, Laura, DomínguezdeMaría, Pablo, Alcántara, Andrés R., 2012. 2-Methyltetrahydrofuran (2-MeTHF): a biomass-derived solvent with broad application in organic chemistry. Chem. Sus. Chem. 5 (8), 1369–1379. https://doi.org/10.1002/cssc.201100780.

Pieper, Henrik, Ommen, Torben, Jensen, Jonas Kjær, Elmegaard, Brian, Brix Markussen, Wiebke, 2020. Comparison of COP estimation methods for large-scale heat pumps used in energy planning. Energy 205, 117994. https://doi.org/10.1016/j.energy.2020.117994. August.

Ramdin, Mahinder, Morrison, Andrew R.T., Groen, Mariette De, et al., 2019. High-pressure electrochemical reduction of CO_2 to formic acid/formate: effect of pH on the downstream separation process and economics. Ind. Eng. Chem. Res 58 (51), 22718–22740. https://doi.org/10.1021/acs.iecr.9b03970.

Rumayor, M., Dominguez-Ramos, A., Irabien, A., 2019a. Environmental and economic assessment of the formic acid electrochemical manufacture using carbon dioxide: influence of the electrode lifetime. Sustain. Product. Consumpt. 18, 72–82. https://doi.org/10.1016/j.spc.2018.12.002. April.

Rumayor, M., Dominguez-Ramos, A., Perez, P., Irabien, A., 2019b. A techno-economic evaluation approach to the electrochemical reduction of CO2 for formic acid manufacture. Journal of CO2 Utilization 34, 490–499. https://doi.org/10.1016/j.jcou.2019.07.024. December.

Salvatore, Danielle, Berlinguette, Curtis P., 2020. Voltage matters when reducing CO_2 in an electrochemical flow cell. ACS Energy Lett. 5 (1), 215–220. https://doi.org/10.1021/acsenergylett.9b02356.

Schlosser, F., Jesper, M., Vogelsang, J., Walmsley, T.G., Arpagaus, C., Hesselbach, J., 2020. Large-scale heat pumps: applications, performance, economic feasibility and industrial integration. Renew. Sustain. Energy Rev. 133, 110219. https://doi.org/10.1016/j.rser.2020.110219. November.

Sharma, Swapnil, Patle, Dipesh S., Gadhamsetti, Akhil Premkumar, Pandit, Sanket, Manca, Davide, Nirmala, G.S, 2018. Intensification and performance assessment of the formic acid production process through a dividing wall reactive distillation column with vapor recompression. Chemic. Eng. Process. - Proc. Intensificat. 123, 204–213. https://doi.org/10.1016/j.cep.2017.11.016. January.

Sinnott, Ray, Towler, Gavin, 2020. Chemical Engineering Design, 6th Edition. Elsevier.

Smith, Wilson A., Burdyny, Thomas, Vermaas, David A., Geerlings, Hans, 2019. Pathways to industrial-scale fuel out of thin air from CO2 electrolysis. Joule 3 (8), 1822–1834. https://doi.org/10.1016/j.joule.2019.07.009.

Somoza-Tornos, Ana, Guerra, Omar J., Crow, Allison M., Smith, Wilson A., Hodge, Bri-Mathias, 2021. Process modeling, techno-economic assessment, and life cycle assessment of the electrochemical reduction of CO2: a review. iScience 24 (7), 102813. https://doi.org/10.1016/j.isci.2021.102813.

Spurgeon, Joshua M., Kumar, Bijandra, 2018. A comparative technoeconomic analysis of pathways for commercial electrochemical CO_2 reduction to liquid products. Energy Environ. Sci. 11 (6), 1536–1551. https://doi.org/10.1039/C8EE00097B.

Thijs, Barbara, Rongé, Jan, Martens, Johan A., 2022. Matching emerging formic acid synthesis processes with application requirements. Green Chem. 24 (6), 2287–2295. https://doi.org/10.1039/D1GC04791D.

U.S. Department of Energy. 2015. Wind Vision: a new era for Wind power in the United States.

U.S. Energy Information Administration. (2025, 04 28). *Electric Power monthly*. Retrieved from https://www.eia.gov/electricity/monthly/epm_table_grapher.php?t=epmt_5_6_a.

Van De Bor, D.M., Infante Ferreira, C.A., Kiss, Anton A., 2014. Optimal performance of compression–Resorption heat pump systems. Appl. Therm. Eng. 65 (1–2), 219–225. https://doi.org/10.1016/j.applthermaleng.2013.12.067.

Van De Bor, D.M., Infante Ferreira, C.A., Kiss, Anton A., 2015. Low grade waste heat recovery using heat pumps and power cycles. Energy 89, 864–873. https://doi.org/10.1016/j.energy.2015.06.030. September.

Van Der Roest, Els, Bol, Ron, Fens, Theo, Wijk, Ad Van, 2023. Utilisation of waste heat from PEM electrolysers – Unlocking local optimisation. Int. J. Hydrogen Energy 48 (72), 27872–27891. https://doi.org/10.1016/j.ijhydene.2023.03.374.

Vannoni, Alberto, Sorce, Alessandro, Traverso, Alberto, Massardo, Aristide Fausto, 2023. Techno-economic optimization of high-temperature heat pumps for waste heat recovery. Energy Conver. Manag. 290, 117194. https://doi.org/10.1016/j.enconman.2023.117194. August.

Vos, Rafaël E., Koper, Marc T.M., 2022. The effect of temperature on the cation-promoted electrochemical CO_2 reduction on gold. Chem. Electro. Chem. 9 (13), e202200239. https://doi.org/10.1002/celc.202200239.

Vos, Rafaël E., Kolmeijer, Kees E., Jacobs, Thimo S., Stam, Ward Van Der, Weckhuysen, Bert M., Koper, Marc T.M., 2023. How temperature affects the selectivity of the electrochemical CO_2 reduction on copper. ACS Catal. 13 (12), 8080–8091. https://doi.org/10.1021/acscatal.3c00706.

Wakerley, David, Lamaison, Sarah, Wicks, Joshua, et al., 2022. Gas diffusion electrodes, reactor designs and key metrics of low-temperature CO2 electrolysers. Nat. Energy. 7 (2), 130–143. https://doi.org/10.1038/s41560-021-00973-9.

Walden, Jasper V.M., Wellig, Beat, Stathopoulos, Panagiotis, 2023. Heat pump integration in non-continuous industrial processes by dynamic pinch analysis targeting. Appl. Energy. 352, 121933. https://doi.org/10.1016/j.apenergy.2023.121933. December.

Wernet, Gregor, Bauer, Christian, Steubing, Bernhard, Reinhard, Jürgen, Moreno-Ruiz, Emilia, Weidema, Bo, 2016. The Ecoinvent Database version 3 (Part I): overview and methodology. Int. J. Life Cycle Assess. 21 (9), 1218–1230. https://doi.org/10.1007/s11367-016-1087-8.

Wu, Zhangxiang, Sha, Li, Yang, Xiaochen, Zhang, Yufeng, 2020. Performance evaluation and working fluid selection of combined heat pump and power generation system (HP-PGs) using multi-objective optimization. Energy Convers. Manage. 221, 113164. https://doi.org/10.1016/j.enconman.2020.113164. October.

Yang, Hongzhou, Kaczur, Jerry J., Sajjad, Syed Dawar, Masel, Richard I., 2017. Electrochemical conversion of CO2 to formic acid utilizing sustainion™ membranes. J. CO2 Utiliz. 20, 208–217. https://doi.org/10.1016/j.jcou.2017.04.011. July.

Yang, Hongzhou, Kaczur, Jerry J., Sajjad, Syed Dawar, Masel, Richard I., 2020. Performance and long-term stability of CO2 conversion to formic acid using a three-compartment electrolyzer design. J. CO2 Utiliz. 42, 101349. https://doi.org/10.1016/j.jcou.2020.101349. December.

Zühlsdorf, Benjamin. 2024. *Annex 58: high-temperature heat pumps*. Heat pump center. https://doi.org/10.23697/2QXE-AV87.

Zhang, Zhongshuo, Xie, Yi, Wang, Ying, 2022. What matters in the emerging application of CO2 electrolysis. Curr. Opinion Electrochem. 34, 101012. https://doi.org/10.1016/j.coelec.2022.101012. August.

Zhang, Weizhe, Zhuo, Yuhang, Hao, Peixuan, et al., 2024. Flexible endothermic or exothermic operation for temperature-oriented alkaline water electrolysis. Cell Reports Physic. Science 5 (4), 101900. https://doi.org/10.1016/j.xcrp.2024.101900.

Zhao, Kaiyin, Jia, Cunqi, Li, Zihao, et al., 2023. Recent advances and future perspectives in carbon capture, transportation, utilization, and storage (CCTUS) technologies: a comprehensive review. Fuel 351, 128913. https://doi.org/10.1016/j.fuel.2023.128913. November.

Zhu, Peng, Wang, Haotian, 2021. High-purity and High-concentration liquid fuels through CO2 electroreduction. Nat. Catal. 4 (11), 943–951. https://doi.org/10.1038/s41929-021-00694-y.